Submitted for the AIAA SciTech Forum and Exposition 11–15 & 19–21 January 2021
Virtual Event
Leading edge vortex formation on finite wings using vortex particles

Hugh J. A. Bird [*], Kiran Ramesh[†],

Aerospace Sciences Division, School of Engineering, University of Glasgow, Glasgow, United Kingdom, G12 8QQ

Shūji Ōtomo [‡] and Ignazio Maria Viola[§]

School of Engineering, Institute for Energy Systems, University of Edinburgh, Edinburgh, United Kingdom, EH9 3FB

The unsteady vortex lattice method is modified with a leading edge wake shedding criterion and a regularized vortex particle wake for application to problems involving leading edge vortices on finite wings. The leading edge vortex structures obtained using this low order method are compared against CFD data for a pitching maneuver. To model seven chord lengths of wing movement, the vortex particle method used $26\,000$ vortex particles and ran in approximately $75\,\text{s}$ on a standard desktop PC.

I. Nomenclature

$\boldsymbol{A}$	=	normal velocity influence matrix
c	=	chord
I	=	number of vortex panels in spanwise direction
J	=	number of vortex panels representing the wing chord
$\boldsymbol{n}$	=	surface normal vector
q	=	velocity regularization function
r	=	radius magnitude
$\boldsymbol{r}$	=	radius vector
t	=	time
$t^* = tU/c$	=	normalized time
Δt	=	time step
$\boldsymbol{u}$	=	local velocity
U	=	free steam velocity
$\mathbf{x}$	=	coordinate
Δx	=	vortex lattice spacing
$\Delta \boldsymbol{x}_P$	=	vortex particle spacing
α	=	angle of attack
$\boldsymbol{\alpha}$	=	vorticity of vortex particle
Γ	=	vorticity per unit length
ζ	=	vorticity regularization function
ρ	=	normalized radius
σ	=	regularization distance
$\boldsymbol{\omega}$	=	vorticity

[*]Graduate Researcher, h.bird.1@research.gla.ac.uk, Student Member AIAA.

[†]Lecturer, Aerospace Science Division, School of Engineering, Kiran.Ramesh@glasgow.ac.uk, Member AIAA

[‡]Ph.D Student, School of Engineering, Institute for Energy Systems, s.otomo@ed.ac.uk

[§]Reader, School of Engineering, Institute for Energy Systems, i.m.viola@ed.ac.uk, Member AIAA

$\omega^* = \omega c / U$ =   normalized vorticity
$\tilde{\omega}$ =   discretized vorticity approximation
Ω =   the set of LEV wake shedding rings

Subscripts

i	=	spanwise subscript
j	=	chordwise subscript
n	=	vortex particle index
m	=	vortex particle index
t	=	belonging to trailing edge wake
l	=	belonging to leading edge wake
LE	=	at the leading edge
crit	=	critical value
wing	=	wing
ext	=	external

II. Introduction

THE leading edge vortex (LEV) is a structure engineers struggle to take advantage of, though it is common in nature [1–3]. This structure is caused by separation at the leading edge of a wing. In unsteady flow conditions, the vortex that forms allows for larger aerodynamic forces than would otherwise be possible in steady flight [4, 5]. This property makes them attractive to engineers aiming to construct oscillating energy harvesting devices [6] and micro air vehicles with flapping wings. These engineers need a means to model LEVs.

The high loads created by LEVs can also be a threat where they are not expected. The designers of flexible high aspect ratio aircraft [7] and wind turbine blades [8] aim to avoid potentially damaging load peaks. These engineers also need to be able to anticipate and potentially model the formation of LEVs.

This can be done with computational fluid dynamics (CFD). In two dimensions, unsteady CFD can accurately model LEVs in a reasonable time-frame without requiring high performance computing (HPC) resources. For applications where the ability to rapidly obtain solutions is more important, low order models can be used. These aim to include only the necessary physics, and as a consequence have a far lower computational cost.

A recent example of such a method is that of Ramesh et al. [9]. A regularized discrete vortex method is combined with thin airfoil theory [10] and a leading edge shedding criterion. This leading edge shedding criterion, based upon the leading edge suction of the airfoil, allows the otherwise incompressible and inviscid model to anticipate not only when a leading edge shear layer should be shed, but also how strong this shear layer should be.

As in 2D, 3D CFD also provides a viable method with which the LEV can be simulated. Naturally the computational cost is far higher however, requiring high performance computing resources. The far greater computational cost may make engineers consider modeling the wing and LEV using strip theory, or to use low order methods that assume no LEV shedding at all [11–13].

In three dimensions, the leading edge vortex structure becomes more complicated. It can merge and interact with the wing tip vortex [14], and have internal spanwise transfer of vorticity. The LEV, as it is convected downstream, also has more complex interactions with both the wing and wake. The LEV often forms an arch structure over the wing that then forms a vortex ring in the wake along with the tip and trailing edge vortices. Similar conclusions were found with both CFD simulations [3, 15–20] and experiments [21–26].

Consequently, a low order model for LEVs on finite wings is desirable. There is a dearth of models for unsteady LEV shedding incorporating 3D effects. Hirato et al. [27] showed that the 2D idea of a critical leading edge suction also applied to the leading edge of finite wings. Consequently, the strength of a leading edge shear layer could be modulated by Ramesh et al.'s LESP criterion. They applied this to an unsteady vortex lattice method including a leading edge vortex sheet [28]. The use of vortex filaments to model the evolution of the LEV creates challenges. Viscosity may be important in the merging of vortex structures in the wake [22] and for the interaction of the LEV with the wing surface. Viscous effects are not easily modeled with vortex filaments. The inability of vortex filaments to adapt to the extreme distortion of the leading edge shear layer is also challenging.

Some of these problems can potentially be solved by modeling the wake using regularized vortex particles instead of filaments. Applicability of the method may be improved by adding viscosity using particle strength exchange schemes,

and the long term stability of the simulation can be improved using particle redistribution schemes and relaxation schemes [29].

This paper proposes an enhanced unsteady vortex lattice method by adopting a vortex particle wake and a leading edge suction based leading edge shedding criterion. The rest of the paper is organized as follows. Vortex particles and vortex filaments are introduced in Sec. III.A and Sec.III.B respectively. This is followed by a description of the unsteady vortex lattice method, its modifications, and the leading edge shedding criterion in Sec. III.D. The final algorithm is then described in Sec. III.E. Next, the CFD method used in this paper is presented in Sec. IV.A, along with validation against experiment in Sec. IV.B. The case used for comparison between CFD and the newly described method is discussed in Sec. IV.C. Section IV.D compares the new method against CFD for vorticity iso-surfaces in 3D, and Sec. IV.E examines a slice of the leading edge vortex at the center of the wing. Conclusions are drawn in Sec. V.

III. Theory

This section starts with a description of vortex particles and vortex filaments, and their interactions. These are presented in Sec. III.A and Sec. III.B respectively. Building upon these basic elements, the vortex lattice structure is then described in Sec. III.C. This groundwork then allows the idea of boundary conditions to be introduced, along with how they might be satisfied, both discussed in Sec. III.D. Finally, an algorithm to simulate the formation of LEVs is presented in Sec. III.E.

A. Vortex particles

Vortex particles, also known as vortons or vortex sticks, are an alternative to vortex filaments. Vortex filaments represent vorticity as the product of vorticity per unit length, Γ, and a direction vector. Vortex particles lump this into a vector valued vorticity $\boldsymbol{\alpha}$.

The vorticity $\tilde{\omega}$ at a point $\boldsymbol{x}$ can be expressed in terms of 'singular' vortex particles as

$$\tilde{\omega}(\boldsymbol{x}, t) = \sum_n \boldsymbol{\alpha}_n(t) \delta(\boldsymbol{x} - \boldsymbol{x}_n(t)) \tag{1}$$

where $\boldsymbol{\alpha_n}$ is the vorticity of nth vortex particle located at $\boldsymbol{x}_n$, t is time and $\delta(\boldsymbol{x})$ is the 3D Dirac delta function. $\tilde{\omega}$ is used to differentiate the discretized vorticity field from the true vorticity field ω. Whilst the ω is divergence free, the approximation $\tilde{\omega}$ generally is not. However, in both cases the velocity field $\boldsymbol{u}$ remains divergence free.

Regularized vortex particles replace the δ-function with a distribution of vorticity, resulting in

$$\tilde{\omega}(\boldsymbol{x}, t) = \sum_n \frac{\boldsymbol{\alpha}_n(t)}{\sigma^3} \zeta\left(\frac{\boldsymbol{x} - \boldsymbol{x}_n(t)}{\sigma}\right) \tag{2}$$

where σ is the regularization distance ('radius') of the vortex particle, and $\zeta(\boldsymbol{x})$ is the regularization function. Normally these regularization functions are radially symmetric, meaning that $\zeta(r/\sigma)$ is used where r is $|\boldsymbol{x} - \boldsymbol{x}_n(t)|$. The regularized distance is referred to as $\rho = r/\sigma$.

Regularized vortex particles are preferred over singular vortex particles since the convergence of the method to the Euler equations can be proven [30]. In practice, regularized particle also make it easier to have stable, long running simulations.

The evolution of the vortex particle field due to induced velocities requires both the local velocity for each vortex particle and its rate of change of vorticity. The strength $\boldsymbol{\alpha}$ of each vortex particle must change to account for stretching of the vortex filaments that a particle field could alternatively be represented by.

To obtain the velocity field and this vortex stretching term, an additional equation related to the regularization of the vortex particle is required. $q(\rho)$, relates to $\zeta(\rho)$ as

$$q(\rho) = \int_0^\rho \zeta(\xi)\xi^2 \, d\xi \tag{3}$$

$$\zeta(\rho) = \frac{1}{\rho^2} \frac{dq}{d\rho}(\rho) \tag{4}$$

From this, the velocity induced by a set of vortex particles can be obtained as

$$\boldsymbol{u}(\boldsymbol{x}, t) = -\sum_n \frac{q\left(\frac{|\boldsymbol{x} - \boldsymbol{x}_n|}{\sigma}\right)}{|\boldsymbol{x} - \boldsymbol{x}_n|^3} (\boldsymbol{x} - \boldsymbol{x}_n) \times \boldsymbol{\alpha}_n \tag{5}$$

3

and the rate of change of vorticity induced on the mth vortex particle can be obtained as

$$\frac{d\boldsymbol{\alpha}_m}{dt} = \sum_n \frac{1}{\sigma^3} \left(q(\rho_{nm}) \frac{\boldsymbol{\alpha}_m \times \boldsymbol{\alpha}_n}{\rho_{nm}^3} + \frac{1}{|\boldsymbol{r}_{nm}|^2} \left(3\frac{q(\rho_{nm})}{\rho_{nm}^3} - \zeta(\rho_{nm}) \right) (\boldsymbol{\alpha}_m \cdot (\boldsymbol{r}_{nm} \times \boldsymbol{\alpha}_n)) \boldsymbol{r}_{nm} \right) \tag{6}$$

where $\boldsymbol{r}_{nm}$ is the vector between the two particles $\boldsymbol{x}_m - \boldsymbol{x}_n$, and ρ_{nm} is $|\boldsymbol{r}_{nm}|/\sigma$.

The vortex stretching equation for ω can be written in three equivalent forms. However, these forms are not equivalent when applied to the discretized field $\tilde{\omega}$. This leads to three possible vortex stretching equations, described as the classical, mixed and transpose schemes. Equation 6 describes the transpose scheme. The classical and mixed schemes are described by Winckelmans and Leonard [29] and by Cottet and Koumoutsakos [31]. Whilst no one scheme is clearly superior, the current work uses the transpose scheme because it conserves the total vorticity of the problem [29].

A choice of regularization scheme must be made. In this paper, the popular Gaussian kernel is used, giving

$$4\pi\zeta_{\text{gaussian}}(\rho) = \sqrt{\frac{2}{\pi}} e^{-\rho^2/2} \tag{7}$$

$$4\pi q_{\text{gaussian}}(\rho) = \text{erf}(\rho/\sqrt{2}) - \rho\zeta_{\text{gaussian}}(\rho) \tag{8}$$

were $\text{erf}(x)$ is the error function as described by Olver et al. [32].

The development of the leading edge vortex results in significant vortex stretching. This creates two problems. Firstly, the stretching of a vortex suggests that the vortex particles representing it move apart. If the vortex particles move so far apart they no longer overlap, the vorticity field they approximate is no longer divergence free. Secondly, the simulation becomes unstable. Redistributing vorticity among a new set of vortex particles that overlap alleviates this problem.

Vortex particle redistribution is covered in Winckelmans et al. [33]. An original set of vortex particles is replaced by a set of particles on a uniform grid with spacing h. The vorticity of the new particles is determined by a redistribution function $\Lambda_{3D}(U, V, W)$. U, V and W are the normalized distances between the new particle and the original particles, given by $U = |\boldsymbol{r}_{nm} \cdot \boldsymbol{e}_x|/\sigma$, $V = |\boldsymbol{r}_{nm} \cdot \boldsymbol{e}_y|/\sigma$ and $W = |\boldsymbol{r}_{nm} \cdot \boldsymbol{e}_z|/\sigma$ where $\boldsymbol{e}_\bullet$ are the basis of the Cartesian system. This 3D redistribution function is obtained from a 1D function $\Lambda(U)$ as $\Lambda_{3D}(U, V, W) = \Lambda(U)\Lambda(V)\Lambda(W)$. Here, a redistribution function that conserves moments up to the third order was used:

$$\Lambda(U) = \begin{cases} \frac{1}{2}(1 - U^2)(2 - U), & \text{if } 0 \leq U \leq 1 \\ \frac{1}{6}(1 - U)(2 - U)(3 - U), & \text{if } 1 \leq U \leq 2 \\ 0, & \text{otherwise} \end{cases} \tag{9}$$

The new vorticity of a newly inserted vortex particle is then obtained as

$$\boldsymbol{\alpha}_m = \sum_n \boldsymbol{\alpha}_n \Lambda(\boldsymbol{r}_{nm}) \tag{10}$$

Since any particle of the original set has its vorticity redistributed locally, the operation can be computed quickly via sparse octree insertion. Repeated redistribution of vorticity can result in a large number of particles with negligible vorticity. Consequently these particles of negligible vorticity are normally removed and their vorticity shared among the remaining particles.

The evolution of the vorticity field is modeled using a Runge-Kutta 2 step scheme [34]. Although a simpler Euler scheme could be used, this leads to increased errors. Implementation of alternates such as second order Adams-Bashforth are complicated by the frequent addition and removal of vortex particles in the presented method.

B. Vortex filaments

Vortex filaments can also be used to represent the vorticity field. Compared to vortex particles, they have the advantage that they can represent a divergence free $\tilde{\omega}$ field, so long as the filaments form a ring.

The velocity induced on a point by a straight fragment of a singular vortex filament is given in Katz and Plotkin [35] as

$$\boldsymbol{u}(\boldsymbol{x}) = \frac{\Gamma}{4\pi} \frac{\boldsymbol{r}_0 \cdot (\hat{\boldsymbol{r}}_1 - \hat{\boldsymbol{r}}_2)}{|\boldsymbol{r}_1 \times \boldsymbol{r}_2|^2} \boldsymbol{r}_1 \times \boldsymbol{r}_2 \tag{11}$$
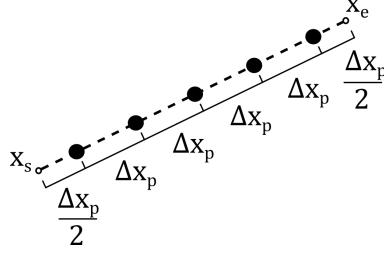
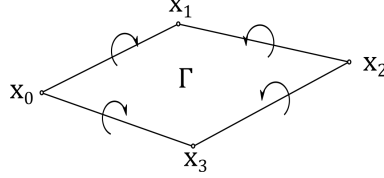**Fig. 1   Placement of vortex particles equivalent to a vortex filament**

Fig. 2   A vortex ring

where Γ is the vorticity per unit length of the vortex filament. If x_s and x_e are the start and end of a vortex filament respectively, $r_0 = x_e - x_s$, $r_1 = x - x_s$ and $r_2 = x - x_e$.

As with vortex filaments, regularized vortex filaments are attractive. Unfortunately, the mathematics related to regularized vortex filaments does not work out so nicely as that for vortex particles. To avoid this problem the vortex filaments can instead be converted into a group of vortex particles. This is show in Fig. 1. Particles are spaced such that the distance between them is equal to or smaller than the regularization radius, resulting a particle spacing of

$$\Delta x_p = \frac{x_e - x_s}{\text{ceil}\left(|x_e - x_s|/\sigma\right) + 1} \tag{12}$$

with each particle having vorticity

$$\alpha = \Gamma \frac{x_e - x_s}{\text{ceil}\left(|x_e - x_s|/\sigma\right) + 1} \tag{13}$$

C. Vortex rings and vortex lattices

A vortex ring is shown in Fig. 2. The quadrilateral vortex ring is comprised of four straight vortex filaments fragments, arranged such that the end of one fragment is the beginning of the next. They share the same vorticity per unit length. As a consequence, the ring has no net vorticity, implicitly satisfying the Kelvin condition. This property is especially useful when solving for vorticity distributions.

Vortex rings are usually used ensemble, most commonly as part of a vortex lattice structure. A vortex lattice representing a surface is shown in Fig. 3. A regular grid of vortex rings is used to represent a surface. The vortex rings are not placed exactly on the geometry of the surface. Instead, the vortex rings are placed a quarter of their length downstream. The boundary condition is normally imposed at the center of the ring. Most often, this boundary condition is that the velocity of the fluid normal to the wing surface matches that of the wing surface.

For the 2D analogue of the an unsteady vortex lattice method, Roesler and Epps [36] note that for the numerical solution to match the linear aerodynamic solution, the timestep must be set as $\Delta t = c/(JU_\infty)$ where J is the number of vortex panels in the chordwise direction. This is possible for rectangular wings. Otherwise the average chord is used.

D. The leading and trailing edge wake

So far, the idea of a vortex lattice representing the wing surface has been presented. However, the trailing edge wake and - in the case of leading edge vortex formation - the leading edge wake must also be considered.

This is done by the addition of more vortex lattices, as described in Katz and Plotkin [35]. A diagram is given in Fig. 4. The vertices of both vortex sheets are convected at their local velocities with the exception of those attached to the wing vortex lattice. In the case of the trailing edge wake, it is attached to the trailing edge vertices. For the leading edge, the first row of rings are attached to the wing vortex lattice leading edge, and the true leading edge of the wing. A
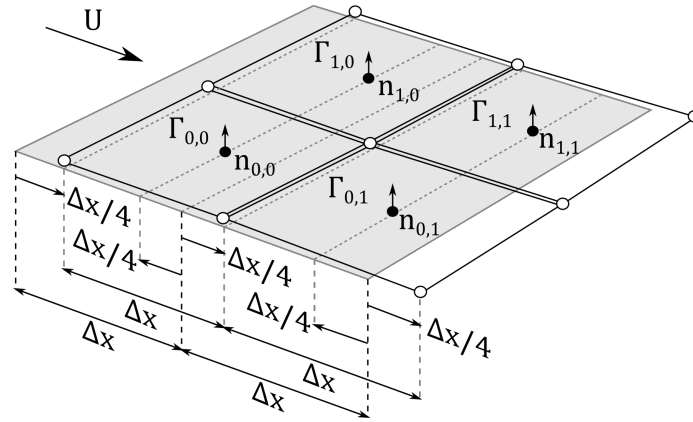
Fig. 3 A vortex lattice representing a surface. The surface is shown in gray.
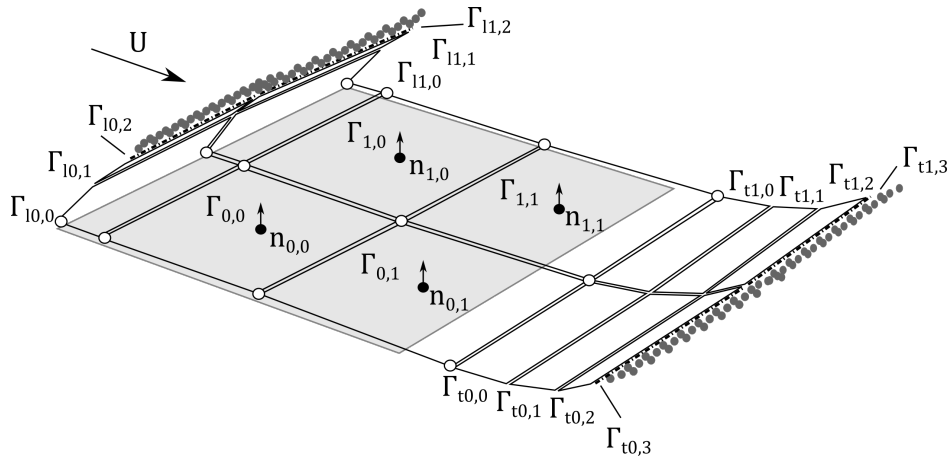

Fig. 4 The vortex lattice representing the wing with both the leading and trailing edge wakes. The white circles represent the constrained geometry. Small lattice buffer regions are shown before the wakes are converted into vortex particles. Dark circles represent vortex particles and the dot-dashed lines represent the edge of a vortex ring that has partially been transformed into vortex particles.

small vortex lattice buffer region (as pioneered by Willis et al. [37]) is used before the wake lattice is converted into vortex particles. This leaves vortex filaments that are not part of the vortex lattice on the trailing edge of the lattice.

Two problems remain. The first problem is how to expand the wake vortex lattice to account for the expansion of the wake with time, and the second is how to obtain the strength of the wake lattice.

To expand the vortex lattice, the wake vortex rings adjacent to the wing lattice are split in two. The location of one of the new vertices is taken as one third of the way from the shedding edge to the next downstream free vertex on the lattice. This technique was pioneered by Ansari et al. [38, 39], and has been widely used for example by Ramesh et al. [9] in 2D and Hirato et al. [28] in 3D. It has the advantage that takes account of both vortex convection and wing motion.

Secondly, the strength of the vortex rings must be obtained. For the trailing edge wake, as the new ring is inserted, it's strength is set to the same value as the adjacent wing vortex lattice ring. Upon the insertion of a wake vortex wing, the trailing edge vorticity of the wing is therefore zero. If the trailing edge wake vortex lattice has ring strengths $\Gamma_{ti,0}$, and the wing and wake are I rings wide, and the chord of the wing is represented by J rings then

$$\Gamma_{ti,0} = \Gamma_{i,J} \quad \text{for } i \in [0, I-1] \tag{14}$$

Obtaining the strength of the leading edge vortex rings is more complex due to non-linear nature of leading edge vortex shedding. The problem is twofold. Firstly, it must be determined whether a leading edge vortex sheet, which rolls up to form the LEV, should be shed. For this, a solution assuming no LEV shedding must be obtained. And secondly, if it is determined that LEV shedding should occur, the strength of the newly shed LEV vortex lattice rings must be obtained simultaneously with those of the wings. The case where no LEV is shed is considered first.

At times where vorticity is not being shed into the leading edge wake, the wing vortex lattice strengths can be solved by satisfying the normal velocity boundary condition on the wing:

$$\{u_{\text{wing}} \cdot n\} = \{u_{\text{ext}} \cdot n\} + [A]\{\Gamma_w\} \tag{15}$$

Here, u_{wing} is the wing surface velocities at the center of the wing lattice vortex rings, n is the wing surface normals at these points and u_{ext} is the externally induced velocity at these points. This external velocity includes the free stream U and the velocity induced by both of the wakes on the assumption that $\Gamma_{li,0} = \Gamma_{li,1}$ for $i \in [0, I-1]$. A is the matrix representing the normal velocity influence of the wing lattice vortex rings strengths $\{\Gamma_w\}$. This is identical to the standard unsteady vortex lattice method, as given by Katz and Plotkin [35].

Accounting for the leading edge vortex requires that the leading edge shedding criterion based on the leading edge suction parameter (LESP) of Ramesh et al. is first introduced [9]. This is the idea that the leading edge of an airfoil can only provide a limited amount of suction to keep flow attached. Consequently, at a critical value of leading edge suction, leading edge separation occurs. This suction can be linked to the singular leading edge vorticity distribution from thin airfoil theory, usually given the coefficient A_0. Therefore, for a given airfoil geometry at a given Reynolds number, there exists a value of $A_{0\text{crit}}$ representing the critical value of leading edge suction parameter, which independent of the kinematics. Whilst this idea is derived from 2D, Hirato et al. found that it is also valid for finite wings [27]. Following Aggarwal [40], A_0 can be related to a critical leading edge filament strength in vortex lattice models as

$$\Gamma_{LEi \text{ crit}} = \frac{A_{0\text{crit}} U c \left[\cos^{-1}\left(1 - \frac{2\Delta x_i}{c_i}\right) + \sin\left(\cos^{-1}\left(1 - \frac{2\Delta x_i}{c_i}\right)\right)\right]}{1.13} \tag{16}$$

where Γ_{LEi} is the vorticity per unit length of the ith leading edge vortex filament of the wing vortex lattice, $\Gamma_{LEi\text{crit}}$ is the critical vorticity per unit length at which it can no longer support more vorticity, Δx_i is the spacing of the vortex lattice in the chordwise direction, and c_i is the wing chord. The constant factor of 1.13 is required for the 2D analogue of this problem to match the result of the LDVM method of Ramesh et al. [9], and matches the result of Hirato et al. [28].

The strength of this is filament is

$$\Gamma_{LEi} = \Gamma_{i,0} - \Gamma_{li,0} \tag{17}$$

Consequently, when $|\Gamma_{LEi}| > \Gamma_{i,0\text{crit}}$, then

$$\Gamma_{li,0} = \Gamma_{i,0} \mp \Gamma_{LEi\text{crit}} \quad \text{such that } \Gamma_{LEi} = \pm\Gamma_{LEi\text{crit}} \tag{18}$$

If this criterion is active for a set of leading edge rings Ω, Eq. 15 is expanded to

$$\{u_{\text{wing}} \cdot n\} = \{u_{\text{ext}-\Omega} \cdot n\} + [A]\{\Gamma\} + [A_\Omega]\{\Gamma_{li,0}\} \tag{19}$$

which can then be solved as a linear system. The velocity induced by the wake, when the strength of the leading edge vortex rings in Ω is set to zero, is given as $\{u_{\text{ext}-\Omega} \cdot n\}$, and the normal velocity induced by the vortex rings in Ω on the wing surface is given by $[A_\Omega]\{\Gamma_{li,0}\}$. Resolving this impacts the leading edge vorticity along the entire wing, suggesting that an iterative approach is required to obtain the correct set of leading edge vortex rings, Ω. In practice, Ω oscillates appears between two possible sets, so the implementation used in this paper assumes that Ω obtained from Eq. 15 is correct.

E. Algorithm

To obtain a solution in time, an algorithm is used:
1) Convect the free wake according to the local velocity.
2) Split the set leading edge vortex rings adjacent to the leading edge, giving the new rings strength equal to the original unsplit rings.
3) Insert a new vortex ring adjacent to the trailing edge in the trailing edge wake and assign it the same strength as adjacent trailing edge wing surface vortex ring.
4) Convert part of the wake vortex lattice sheets into vortex particles.
5) Solve for the the wing surface vortex ring strengths, assuming no leading edge shedding.
6) The set of leading edge locations where the shedding criterion is activated is Ω. Recalculate the wing surface ring strengths on this assumption.

Having defined a method, the results obtained using it can now be compared to CFD. For convenience, the method will be referred to as the Vortex Formation on Finite Leading Edge, or VoFFLE, method.

IV. Results

In this section, VoFFLE is compared to results obtained from CFD simulations for a rectangular aspect ratio 3 wing pitching about its leading edge. The CFD method is described in Sec. IV.A, and validated in Sec. IV.B against experiments for a wing oscillating in heave. The results for the vorticity fields of the VoFFLE method and the CFD results are compared for a case described in Sec. IV.C, with results presented in Sec. IV.D and Sec. IV.E.

A. Numerical methods

The open-source CFD toolbox OpenFOAM is used to perform high-fidelity 3D computations of unsteady fluid dynamics at a Reynolds number of 10 000. A body-fitted computational mesh is moved in accordance with prescribed rate laws, and the time-dependent incompressible Navier-Stokes are solved using a finite-volume method. The transient terms are discretized using a second-order backward implicit scheme, while second-order, limited Gaussian integration schemes are used for the gradient, divergence and Laplacian terms. The pressure implicit with splitting of operators (PISO) algorithm is employed to achieve pressure-velocity coupling and the Spalart-Allmaras (SA) turbulence model [41] is used for turbulence closure. This turbulance model is chosen for this problem because of extensive previous experience in applying it successfully for unsteady, separated and vortex-dominated flows at $Re = 10\,000$ such as those considered in this research [9, 42]. The trip terms of the original SA model are turned off, and for the low Reynolds number cases considered in this research, the effects of the turbulence model are confined to the shed vortical structures and wake.

The chord length $c = 0.1$ m. The O-mesh has 116 cells chordwise, with increased resolution near the leading and trailing edges. There are 105 cells in the spanwise direction. The spanwise domain extends 4 chord lengths beyond the wingtip with an average spacing of 21 cells per chord length in this region. In the wall-normal direction, cell spacing begins at 1.5×10^{-5} m next to the wall ($y+ < 1$) and extends a distance of 11.5 chord lengths away from the wing with an average density of 16.3 cells per chord length. The simulations were carried out at a free stream velocity $U = 0.1$ m/s and kinematic viscosity 10^{-6} m^2/s.

B. Validation of CFD against experiment

The CFD results were validated against an experiment performed in the water flume at the University of Edinburgh.

A wing was 3D printed with chord length $c = 100$ mm, aspect ratio $Æ = 3$ and a NACA0008 airfoil section. The freestream velocity was fixed at 0.1 m/s, resulting in the chord based Reynolds number of 10 000. The plunging foil rig, depicted by Fig. 5, consists of two linear motors (LinMot, PS01-23x80F-HP-R20) connected with each other via a linkage system and a coupler plate.
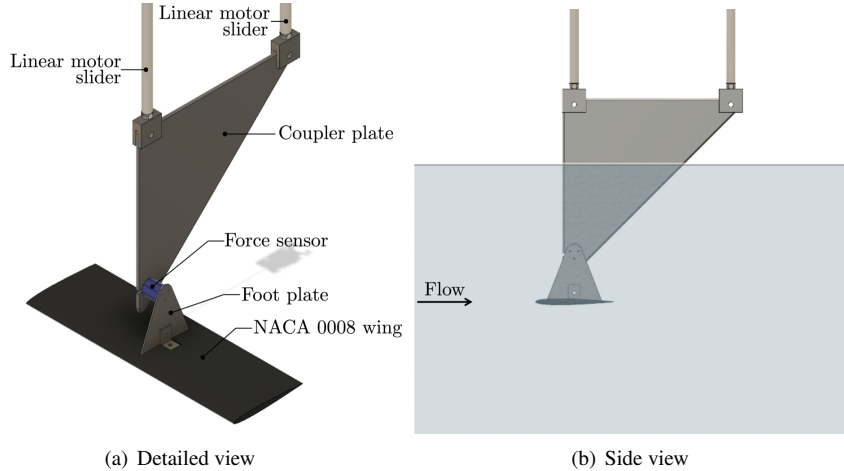
(a) Detailed view   (b) Side view

Fig. 5 Test section and experimental setup

Direct force measurements are conducted. A six-axis force/torque sensor (ATI Inc., Nano-17 IP68) is mounted between the coupler plate and the foot plate. The sensor is capable of measuring forces in the plane of the wing cross section up to ± 25 N, and ± 35 N in the orthogonal direction, and moments up to ± 250 N m around the three axes with a resolution of $1/160$ N for the forces and $1/32$ N m for the moments. LabVIEW is used to trigger the prescribed motor kinematics through a digital output device and also to start recording forces for a synchronized measurement through a DAQ board. A sampling frequency of 10 kHz is used to record the forces, which are then filtered in three steps. Firstly, a fourth-order Butterworth low-pass filter with a cutting frequency of 75 Hz was applied. Then the data was smoothed with a 200 points moving average. The last step is a sixth-order Chebyshev II low-pass filter with -20 dB attenuation in the stopband. This three-step filtering method can preserve load spikes. Phase-averaging is applied for 20 periods.

Particle image velocimetry (PIV) is used to perform flowfield analysis . A double pulsed Nd:YAG laser (New Wave Research, Solo PIV, 532 nm, 200 mJ) is used to illuminated the plane at 1/4 of the span of the wing, with silver coated hollow glass spheres (Potters Industries, 10 μm) used as seeding. Images are then obtained by a CCD camera (IMPERX, B2020 equipped with Nikon 50 mm lens) with a resolution of 2056 pix $\times$ 2060 pix. Velocity vectors are computed using adaptive multi-pass cross-correlation, with a first interrogation window of 64 pix $\times$ 64 pix, and a final interrogation window of 32 pix $\times$ 32 pix, and an overlap of 50% (DaVis, LaVision Inc.). 30 periods of Gaussian filtered PIV data are used for phase-averaging.

The validation case was that of the aspect ratio 3 wing oscillating sinusoidally at normalized amplitude $h_0^* = 0.5$ and chord reduced frequency $k = 0.4$, such that $z = h_0^* c \cos(2Ukt/c)$. This amplitude is sufficient to cause the formation of leading edge vortices. A comparison of the lift coefficients obtained from the CFD and the experiment are shown in Fig. 6. PIV data is compared at $t/T = [1/8, 3/16, 3/8, 1/2]$ - critical points that demonstrate the development of LEV at the quarter span on the wing. This is shown in Fig. 7.

The CFD and experiment are in good agreement for the lift coefficients. The PIV data also agrees well with the CFD. Both methods agree well with the formation of the leading edge separation bubble between $t/T = 1/8$ and $t/T = 3/16$. At $t/T = 3/8$, the angle of the form of the leading edge shear layer matches, along with the approximate shape of the LEV region. By $t/T = 1/2$, the methods agree that the vortex structure has been convected downstream, and remains attached to the surface of the airfoil.

C. Comparison case setup

An aspect ratio 3 wing undergoing leading edge pitch kinematics was studied. As was the case for the validation, the wing had a NACA0008 airfoil and squared off wing tips. The free stream velocity U was 0.1 m s^{-1}, and the chord length was 0.1 m. The canonical pitch up-down ramp given by Ol et al. [43] was used to control angle of attack, with a maximum amplitude of $25°$:

$$\alpha = \frac{K}{a}\left[\frac{\cosh(aU(t-t_1)/c)\cosh(aU(t-t_4)/c)}{\cosh(aU(t-t_2)/c)\cosh(aU(t-t_3)/c)}\right] \tag{20}$$
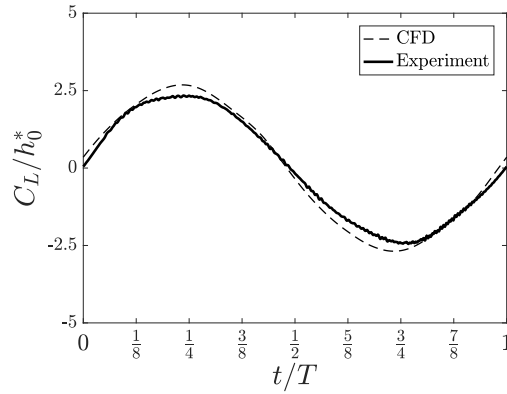
9

Fig. 6 A comparison of the lift coefficients obtained from CFD and experiment for a rectangular aspect ratio 3 wing oscillating in heave at normalized amplitude $h_0^* = 0.5$ and reduced frequency $k = 0.4$.
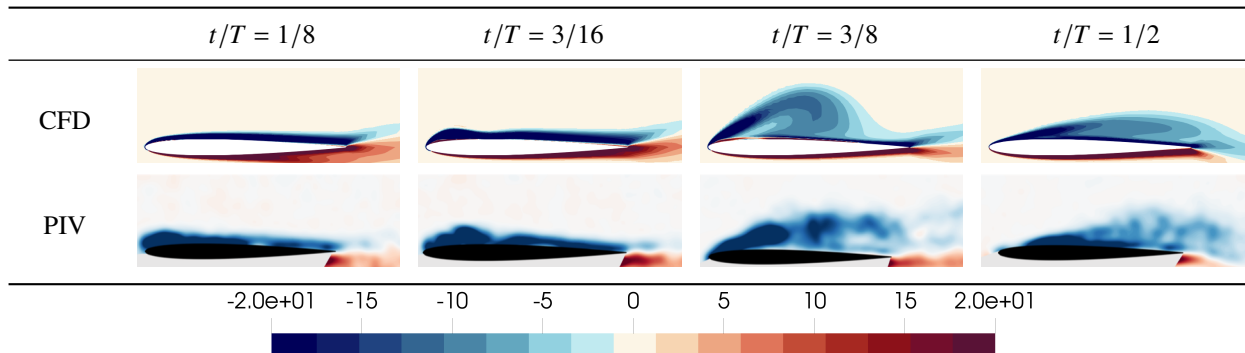

Fig. 7 A comparison of experimental and CFD quarter span normalized spanwise vorticity $\omega_y c/U$ distributions for rectangular aspect ratio 3 wings oscillating sinusoidally in heave at chord reduced frequency $k = 0.4$ and $h_0^* = 0.5$.

10

with $a = \pi^2/(4(t_2 - t_1)(1 - \eta))$ and K set to give $\alpha_{max} = 25°$. Here the parameters $t_1 = 1$, $t_2 = 3$, $t_3 = 4$ and $t_4 = 6$ were used, along with a smoothing parameter $\eta = 0.5$.

The VoFFLE method represented the wing as a flat vortex lattice of uniform spacing. There were 20 rings in the chordwise direction and 45 rings in the spanwise direction. In accordance with the work of Roesler and Epps [36], a timestep $\Delta t = 0.05$ was used. Gaussian regularization was used with regularization distance of $\sigma = 1.5U\Delta t$, following Ramesh et al. [9]. This was combined with a second order Runge-Kutta scheme for the vortex particle field evolution. On even timesteps, the Λ_3 particle redistribution scheme described in the theory section was applied. The critical value of the leading edge suction parameter was taken as 0.16. This was obtained by comparing the results of 2D CFD to those of a large thin airfoil theory as described by Ramesh et al. [9].

To complete the 7 chord lengths of convection required, the VoFFLE method required 73 s on a desktop computer, resulting in approximately 26 000 wake particles after 7 s of simulation time, equivalent to 7 chord lengths of convection. This compares to 2, 200 core hours on an HPC system. A naive direct method was used for the N-body interaction, albeit accelerated with a graphics processing unit. The method is mesh-free, consequently also saving significant time during pre-processing compared to traditional CFD techniques. Since there is no volume mesh to be saved, the space requirements to save the state of a simulation is also relatively small.

To compare the CFD and VoFFLE result, the vorticity iso-surface for the two methods will first be examined in Sec. IV.D, before the vorticity at the center of the wing and the form of the LEV are examined in Sec. IV.E.

D. Comparison of vorticity fields

The vorticity field for both the CFD and the VoFFLE method are shown in Fig. 8. This is visualized as an iso-surface of vorticity magnitude for $|\omega^*| = |\omega c/U| = 1$.

Four points in time are shown, normalized as $t^* = tU/c$. Firstly time $t^* = 3$ is midway through the pitch up ramp, showing the initial LEV formation. Secondly, at time $t^* = 4$, the wing is reaching the top of the pitch ramp and the LEV is well established. At time $t^* = 5$, the wing is returning to zero angle of attack. The LEV has grown larger than at $t^* = 4$, an is no longer attached to the leading edge corners of the wing. And finally at time $t^* = 6$, the angle of attack is now much smaller, and the LEV is no longer being shed. It is convected off the surface of the wing.

Comparing the CFD and the VoFFLE method at $t^* = 3$, the tip vortex is prominent in both predictions. For the CFD this vortex extends to the leading edge, but in the VoFFLE method result, it does not since tip separation is not modeled. In both cases a leading edge vortex is forming. In the CFD, the LEV forms a bubble at the leading edge. For the VoFFLE method, the LEV has been convected downstream. In both cases, the LEV becomes larger toward the center of the wing due to the downwash created by the wing-tip vortex. The VoFFLE method correctly captures that the LEV forms in the center of the wing initially and spreads, but separation from the wing surface is less prominent than predicted by CFD.

At time $t^* = 4$, the angle of attack has increased and the LEV is more prominent in both cases. Again, the CFD predicts a better attached LEV than the VoFFLE method. The VoFFLE method over-predicts the extent to which the LEV is convected downstream.

At time $t^* = 5$, the LEV is no longer pinned to the leading edge corners of the wing. An arch shaped vortex is formed, with its feet on the wing surface. This is found in both the CFD and the VoFFLE method, although the VoFFLE method predicts that the vortex arch has been carried further downstream.

Finally, at time $t^* = 6$ the LEV shed during the pitching motion has separated from the wing surface and is now in the wake. As is the case for all time steps, it has been carried further downstream in the VoFFLE method result than in the CFD result.

The VoFFLE method correctly captured some key features of the problem. The LEV was correctly shed and carried downstream, albeit more quickly than the CFD result. The correct variation of the LEV with respect to span was shown. And importantly, the LEV could be completely shed from the wing.

The largest difference between the CFD and VoFFLE results will be examined in the next section where the LEV at the center of the wing will be examined.

E. The LEV at the wing center

The LEV at the center of the wing is visualized by taking a slice showing the spanwise vorticity. This is shown in Fig. 9.

Five instantaneous vorticity fields are shown. The first is at $t^* = 2.5$, prior to LEV formation. Both the CFD and VoFFLE method show very similar trailing edge wakes. The VoFFLE method assumes inviscid flow, and its semi-Lagrangian nature results in very little dissipation of vorticity as it is convected. Consequently, the CFD results
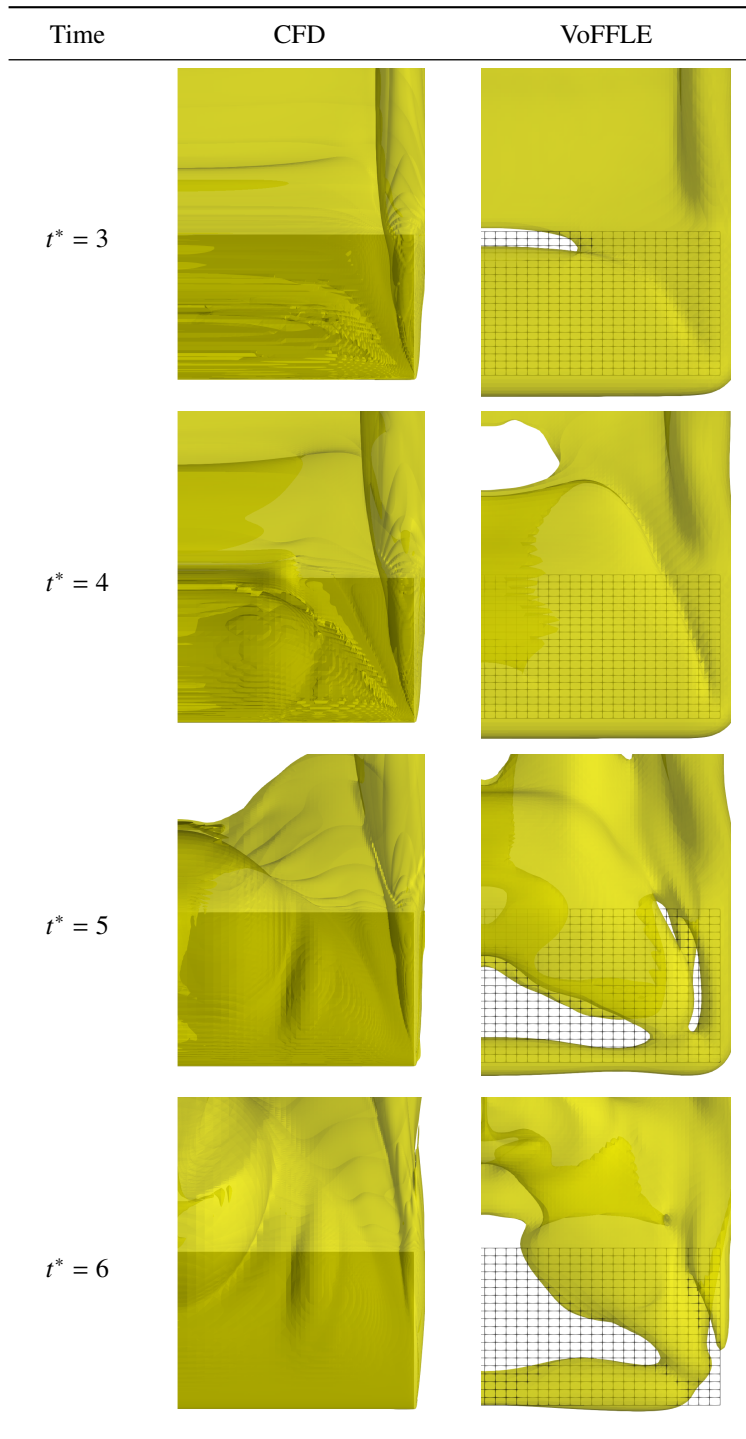
11

Fig. 8 **A comparison of vorticity magnitude iso-surfaces for $|\omega c/U| = 1$ for an aspect ratio 3 wing undergoing a pitch up-down ramp motion.**
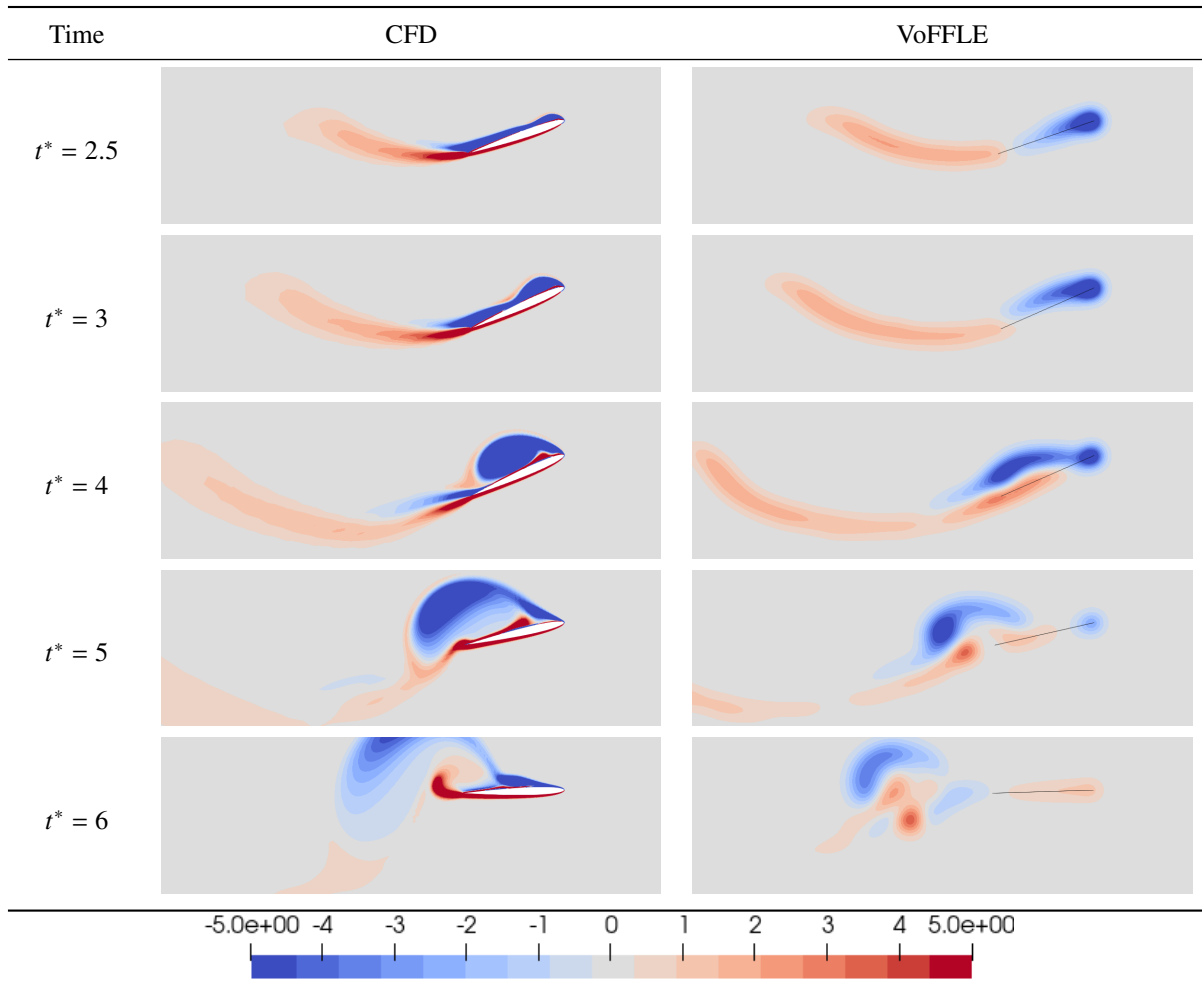
Time	CFD	VoFFLE
$t^* = 2.5$		
$t^* = 3$		
$t^* = 4$		
$t^* = 5$		
$t^* = 6$		

-5.0e+00 -4   -3   -2   -1   0   1   2   3   4   5.0e+00

Fig. 9   **A comparison of normalized spanwise vorticity $\omega_y c/U$ at the center of an aspect ratio 3 wing undergoing a pitch up-down ramp motion.**

show diffusion of the vorticity in the wake and the VoFFLE method does not. The CFD results also show the formation of a laminar separation bubble. The VoFFLE method cannot capture this fine detail for two reasons. Firstly, the formation of the separation bubble is a viscous phenomena. The VoFFLE method captures leading edge phenomena explicitly using the LESP criterion. Secondly, the VoFFLE method cannot model small features. The use of a vortex lattice for wing assumes that the wing in thin, and that features on the scale of the wing's thickness can be neglected. Also, features smaller than the particle regularization distance cannot be resolved.

Between time $t^* = 2.5$ and $t^* = 3$ both models predict that leading edge separation occurs. In the CFD, the leading edge shear layer rolls up to form an LEV. However, in the VoFFLE method, the leading edge shear layer is not sufficiently strong for roll up to occur, and it is instead convected over the wing surface.

This trend continues at time $t^* = 4$. In the CFD, a large attached LEV has formed. A more concentrated LEV is beginning to form in the VoFFLE method, but it is not comparable to that of the CFD. The LEV remains attached to the leading edge via the shear layer in both the CFD and VoFFLE method.

At time $t^* = 5$, the CFD predicts that the leading edge vortex is no longer attached to the wing surface and has been carried downstream such that it is over the trailing edge. However, unlike the VoFFLE prediction, it remains attached to the leading edge via a shear layer. The VoFFLE method predicts that the LEV has separated from the leading edge and has been carried beyond the trailing edge of the wing. The counter-vortex formed as it passes the trailing edge is also visible.

By time $t^* = 6$, in both the CFD and the VoFFLE method the LEV is no longer close to the wing. In the CFD, the LEV is still attached to the wing by a weak shear layer. In the VoFFLE method, the wake contains the LEV, the counter vortex formed as it passed over the wing's trailing edge and additional spurious vorticity. This spurious vorticity is due to the long-term instability of the inviscid vortex particle method used here.

V. Conclusions

A method by which vortex particles can be used to model leading edge vortex formation on a finite wing was developed by adapting an unsteady vortex lattice method with a leading edge wake, transitioning parts of the wake to regularized vortex particles and introducing a leading edge separation criterion.

The current method correctly predicted the timing of the onset of LEV formation, modeled the separation of the LEV from the wing, and reflected the trends of the CFD solution used for comparison, although the details of predicted solution did not match. The vortex particle based model could be run in just over a minute for a test case on a desktop PC, compared to 2, 200 core hours on HPC resources for the 3D CFD. Additionally, it required minimal pre-processing and a more manageable data set for post-processing.

The model could be improved with a better method to computer the leading edge shear layer strength, the addition of shear layers simulating separation at the wing tip and viscous interaction in the wake (possible using particle strength exchange) to aid the stability of the method. Consequently, it has the potential of providing a convenient alternative to CFD for fast, low-cost simulations of finite wings shedding LEVs.

VI. Acknowledgments

References

[1] Birch, J. M., and Dickinson, M. H., "Spanwise flow and the attachment of the leading-edge vortex on insect wings," *Nature*, Vol. 412, No. 6848, 2001, pp. 729–733. doi:10.1038/35089071.

[2] Oh, S., Lee, B., Park, H., Choi, H., and Kim, S.-T., "A numerical and theoretical study of the aerodynamic performance of a hovering rhinoceros beetle (Trypoxylus dichotomus)," *Journal of Fluid Mechanics*, Vol. 885, 2019. doi:10.1017/jfm.2019.962.

[3] Blondeaux, P., Fornarelli, F., Guglielmini, L., Triantafyllou, M. S., and Verzicco, R., "Numerical experiments on flapping foils mimicking fish-like locomotion," *Physics of Fluids*, Vol. 17, No. 11, 2005, p. 113601. doi:10.1063/1.2131923.

[4] Ford, C. W. P., and Babinsky, H., "Lift and the leading-edge vortex," *Journal of Fluid Mechanics*, Vol. 720, 2013, pp. 280–313. doi:10.1017/jfm.2013.28.

[5] Calderon, D. E., Wang, Z., and Gursul, I., "Lift-Enhancing Vortex Flows Generated by Plunging Rectangular Wings with Small Amplitude," *AIAA Journal*, Vol. 51, No. 12, 2013, pp. 2953–2964. doi:10.2514/1.j052600.

[6] Rostami, A. B., and Armandei, M., "Renewable energy harvesting by vortex-induced motions: Review and benchmarking of technologies," *Renewable and Sustainable Energy Reviews*, Vol. 70, 2017, pp. 193–214. doi:10.1016/j.rser.2016.11.202.

[7] Wang, Z., Chen, P. C., Liu, D. D., and Mook, D. T., "Nonlinear-Aerodynamics/Nonlinear-Structure Interaction Methodology for a High-Altitude Long-Endurance Wing," *Journal of Aircraft*, Vol. 47, No. 2, 2010, pp. 556–566. doi:10.2514/1.45694.

[8] Hansen, M., Sørensen, J., Voutsinas, S., Sørensen, N., and Madsen, H., "State of the art in wind turbine aerodynamics and aeroelasticity," *Progress in Aerospace Sciences*, Vol. 42, No. 4, 2006, pp. 285–330. doi:10.1016/j.paerosci.2006.10.002.

[9] Ramesh, K., Gopalarathnam, A., Granlund, K., Ol, M. V., and Edwards, J. R., "Discrete-vortex method with novel shedding criterion for unsteady aerofoil flows with intermittent leading-edge vortex shedding," *Journal of Fluid Mechanics*, Vol. 751, 2014, pp. 500–538. doi:10.1017/jfm.2014.297.

[10] Ramesh, K., Gopalarathnam, A., Edwards, J. R., Ol, M. V., and Granlund, K., "An unsteady airfoil theory applied to pitching motions validated against experiment and computation," *Theoretical and Computational Fluid Dynamics*, Vol. 27, No. 6, 2013, pp. 843–864. doi:10.1007/s00162-012-0292-8.

[11] Ramesh, K., Monteiro, T. P., Silvestre, F. J., Bernardo, A., aes Neto, G., de Souza Siqueria Versiani, T., and da Silva, R. G. A., "Experimental and Numerical Investigation of Post-Flutter Limit Cycle Oscillations on a Cantilevered Flat Plate," *International Forum on Aeroelasticity and Structural Dynamics 2017*, 2017. URL http://eprints.gla.ac.uk/154722/.

[12] Bird, H. J. A., and Ramesh, K., "Theoretical and computational studies of a rectangular finite wing oscillating in pitch and heave," *6th European Conference on Computational Mechanics (ECCM 6) 7th European Conference on Computational Fluid Dynamics (ECFD 7)*, International Centre for Numerical Methods in Engineering, 2018.

[13] Bird, H. J. A., Otomo, S., Ramesh, K., and Viola, I. M., "A Geometrically Non-Linear Time-Domain Unsteady Lifting-Line Theory," *AIAA Scitech 2019 Forum*, American Institute of Aeronautics and Astronautics, 2019. doi:10.2514/6.2019-1377.

[14] Shyy, W., Trizila, P., Kang, C.-K., and Aono, H., "Can Tip Vortices Enhance Lift of a Flapping Wing?" *AIAA Journal*, Vol. 47, No. 2, 2009, pp. 289–293. doi:10.2514/1.41732.

[15] Dong, H., Mittal, R., and Najjar, F. M., "Wake topology and hydrodynamic performance of low-aspect-ratio flapping foils," *Journal of Fluid Mechanics*, Vol. 566, 2006, p. 309. doi:10.1017/s002211200600190x.

[16] Visbal, M., Yilmaz, T. O., and Rockwell, D., "Three-dimensional vortex formation on a heaving low-aspect-ratio wing: Computations and experiments," *Journal of Fluids and Structures*, Vol. 38, 2013, pp. 58–76. doi:10.1016/j.jfluidstructs.2012.12.005.

[17] Hord, K., and Lian, Y., "Leading Edge Vortex Circulation Development on Finite Aspect Ratio Pitch-Up Wings," *AIAA Journal*, Vol. 54, No. 9, 2016, pp. 2755–2767. doi:10.2514/1.j053911.

[18] Visbal, M. R., "Unsteady flow structure and loading of a pitching low-aspect-ratio wing," *Physical Review Fluids*, Vol. 2, No. 2, 2017. doi:10.1103/physrevfluids.2.024703.

[19] Visbal, M. R., and Garmann, D. J., "Dynamic Stall of a Finite-Aspect-Ratio Wing," *AIAA Journal*, Vol. 57, No. 3, 2019, pp. 962–977. doi:10.2514/1.j057457.

[20] Venkata, S. K., and Jones, A. R., "Leading-Edge Vortex Structure over Multiple Revolutions of a Rotating Wing," *Journal of Aircraft*, Vol. 50, No. 4, 2013, pp. 1312–1316. doi:10.2514/1.c032128.

[21] Ellenrieder, K. D. V., Parker, K., and Soria, J., "Flow structures behind a heaving and pitching finite-span wing," *Journal of Fluid Mechanics*, Vol. 490, 2003, pp. 129–138. doi:10.1017/s0022112003005408.

[22] Buchholz, J. H. J., and Smits, A. J., "On the evolution of the wake structure produced by a low-aspect-ratio pitching panel," *Journal of Fluid Mechanics*, Vol. 546, No. -1, 2005, p. 433. doi:10.1017/s0022112005006865.

[23] Yilmaz, T. O., and Rockwell, D., "Three-dimensional flow structure on a maneuvering wing," *Experiments in Fluids*, Vol. 48, No. 3, 2009, pp. 539–544. doi:10.1007/s00348-009-0772-9.

[24] Taira, K., and Colonius, T., "Three-dimensional flows around low-aspect-ratio flat-plate wings at low Reynolds numbers," *Journal of Fluid Mechanics*, Vol. 623, 2009, p. 187. doi:10.1017/S0022112008005314.

[25] Yilmaz, T. O., and Rockwell, D., "Flow structure on finite-span wings due to pitch-up motion," *Journal of Fluid Mechanics*, Vol. 691, 2011, pp. 518–545. doi:10.1017/jfm.2011.490.

[26] Calderon, D. E., Wang, Z., Gursul, I., and Visbal, M. R., "Volumetric measurements and simulations of the vortex structures generated by low aspect ratio plunging wings," *Physics of Fluids*, Vol. 25, No. 6, 2013, p. 067102. doi:10.1063/1.4808440.

[27] Hirato, Y., Shen, M., Gopalarathnam, A., and Edwards, J. R., "Flow Criticality Governs Leading-Edge-Vortex Initiation on Finite Wings in Unsteady Flow," *Journal of Fluid Mechanics*, 2020. Submitted for publication.

[28] Hirato, Y., Shen, M., Gopalarathnam, A., and Edwards, J. R., "Vortex-Sheet Representation of Leading-Edge Vortex Shedding from Finite Wings," *Journal of Aircraft*, 2019, pp. 1–15. doi:10.2514/1.c035124.

[29] Winckelmans, G., and Leonard, A., "Contributions to Vortex Particle Methods for the Computation of Three-Dimensional Incompressible Unsteady Flows," *Journal of Computational Physics*, Vol. 109, No. 2, 1993, pp. 247–273. doi:10.1006/jcph. 1993.1216.

[30] Beale, J. T., and Majda, A., "Vortex methods. I. Convergence in three dimensions," *Mathematics of Computation*, Vol. 39, No. 159, 1982, pp. 1–1. doi:10.1090/s0025-5718-1982-0658212-5.

[31] Cottet, G.-H., and Koumoutsakos, P. D., *Vortex Methods*, Cambridge University Press, 2004. URL `https://www.ebook.de/de/product/4248027/georges_henri_cottet_petros_d_koumoutsakos_vortex_methods.html`.

[32] Olver, F. W., Lozier, D. W., Boisvert, R. F., and Clark, C. W., *NIST Handbook of Mathematical Functions Paperback and CD-ROM*, Cambridge University Press, 2010.

[33] Winckelmans, G., Cocle, R., Dufresne, L., and Capart, R., "Vortex methods and their application to trailing wake vortex simulations," *Comptes Rendus Physique*, Vol. 6, No. 4-5, 2005, pp. 467–486. doi:10.1016/j.crhy.2005.05.001.

[34] Press, W. H., Teukolsky, S. A., Vetterling, W. T., and Flannery, B. P., *Numerical Recipes in C*, 2nd ed., Cambridge University Press, 1992.

[35] Katz, J., and Plotkin, A., *Low Speed Aerodynamics*, 2nd ed., Cambridge University Press, 2001.

[36] Roesler, B. T., and Epps, B. P., "Discretization Requirements for Vortex Lattice Methods to Match Unsteady Aerodynamics Theory," *AIAA Journal*, Vol. 56, No. 6, 2018, pp. 2478–2483. doi:10.2514/1.j056400.

[37] Willis, D. J., Peraire, J., and White, J. K., "A combined pFFT-multipole tree code, unsteady panel method with vortex particle wakes," *International Journal for Numerical Methods in Fluids*, Vol. 53, No. 8, 2007, pp. 1399–1422. doi:10.2514/6.2005-854.

[38] Ansari, S. A., Żbikowski, R., and Knowles, K., "Non-linear unsteady aerodynamic model for insect-like flapping wings in the hover. Part 1: Methodology and analysis," *Proceedings of the Institution of Mechanical Engineers, Part G: Journal of Aerospace Engineering*, Vol. 220, No. 2, 2006, pp. 61–83. doi:10.1243/09544100jaero49.

[39] Ansari, S. A., Żbikowski, R., and Knowles, K., "Non-linear unsteady aerodynamic model for insect-like flapping wings in the hover. Part 2: Implementation and validation," *Proceedings of the Institution of Mechanical Engineers, Part G: Journal of Aerospace Engineering*, Vol. 220, No. 3, 2006, pp. 169–186. doi:10.1243/09544100jaero50.

[40] Aggarwal, S., "An Invicid Numerical Method for Unsteady Flows Over Airfoils and Wings to Predict the Onset of Leading Edge Vortex Formation," Master's thesis, North Carolina State University, 2013. doi:https://oatd.org/oatd/record?record=oai%5C%3Arepository.lib.ncsu.edu%5C%3A1840.16%5C%2F9084, retrieved 05/06/2020.

[41] Spalart, P., and Allmaras, S., "A one-equation turbulence model for aerodynamic flows," *30th Aerospace Sciences Meeting and Exhibit*, American Institute of Aeronautics and Astronautics, 1992. doi:10.2514/6.1992-439, AIAA Paper 1992-0439.

[42] McGowan, G. Z., Granlund, K., Ol, M. V., Gopalarathnam, A., and Edwards, J. R., "Investigations of Lift-Based Pitch-Plunge Equivalence for Airfoils at Low Reynolds Numbers," *AIAA Journal*, Vol. 49, No. 7, 2011, pp. 1511–1524. doi:10.2514/1.j050924.

[43] Ol, M., Altman, A., Eldredge, J., Garmann, D., and Lian, Y., "Résumé of the AIAA FDTC Low Reynolds Number Discussion Group's Canonical Cases," *48th AIAA Aerospace Sciences Meeting Including the New Horizons Forum and Aerospace Exposition*, American Institute of Aeronautics and Astronautics, 2010. doi:10.2514/6.2010-1085, AIAA 2010-1085.